Electronic supplementary information

Progressive Bovine Sperm Separation Using Parallelized Microchamber-based Microfluidics

*Mohammad Yaghoobi, Morteza Azizi, Amir Mokhtare, Alireza Abbaspourrad**

M.Y. Author 1, M.A. Author 2, A.M. Author 3, A.A. Author 4

Food Science Department, College of Agriculture and Life Sciences, Cornell University, Ithaca, NY 14853, USA.

E-mail: **alireza@cornell.edu**

1. Optimization of the loaded volume

The basic geometry of the chip is shown in the above picture and the area confined in the red rectangle is the repetitive building block. We suppose that the confined shaded area over the area of the red rectangle should be optimized in order to maximize the volume of the loaded sample. The radius of the microchambers are assumed as R and the minimum width of the unshaded area is assumed to be s_x in the x direction and s_y in the y direction. This width is crucial for the purpose of maintaining the intact bonding of the PDMS to glass while pressure is exerted at the inlet in the loading process. The restricted shaded area, A_{sh}, is roughly composed of two semi-circles and two rectangles.

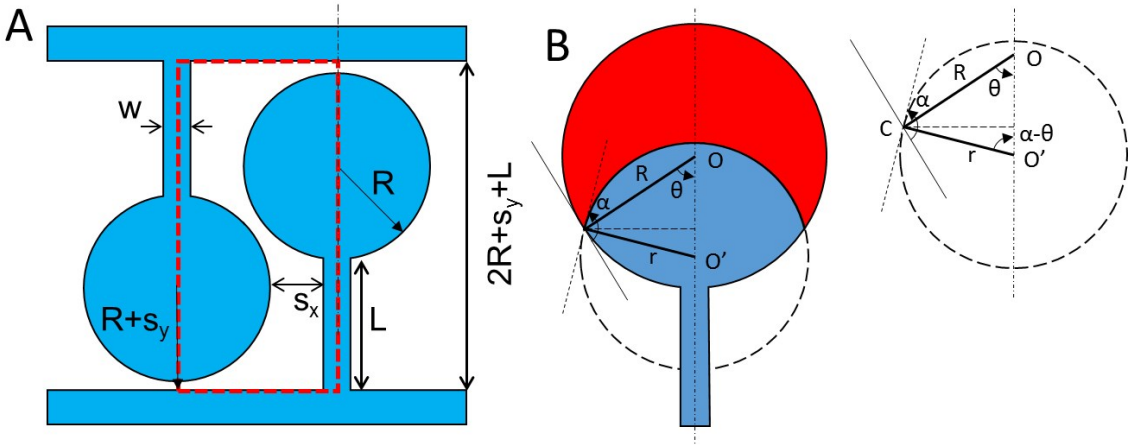

Figure S1. (A) The schematic of the microchannel arrays and dimensions. (B) The schematic diagram of loading process. The dimensions and parameters.

$$A_{sh} = \pi R^2 + wL$$

$$\eta = \frac{A_{sh}}{A_{total}} = \frac{\pi R^2 + wL}{(L + s_y + 2R)(R + s_x + w)}$$

The optimization here has two restrictions which indicates the edges of the rectangle are given and have values of χ_0 and χ_1 for horizontal and vertical edges, respectively.

$$L + s_y + 2R = \chi_0$$

$$R + s_x + w = \chi_1$$

Differentiating the η and restrictions gives us the condition under which the η becomes maximum.

$$\begin{cases} d\eta = 2\pi R dR + w dL + L dw = 0 \\ dL + 2dR = 0 \\ dw + dR = 0 \end{cases}$$

rearrangement of the equation above narrows it down to the optimal value of the microchambers' radius.

$$R_{opt} = \frac{2w_{opt} + L_{opt}}{2\pi}$$

The subscript opt indicates the optimal value of the parameters here. Now by substituting this in the set of the equation of the χ_0 and χ_1:

$$\begin{cases} L + s_y + 2\dfrac{2w + L}{2\pi} = \chi_{0} \\ \dfrac{2w + L}{2\pi} + s_x + w = \chi_1 \end{cases} \xrightarrow{yields} \begin{bmatrix} L \\ w \end{bmatrix} = \begin{bmatrix} \dfrac{\pi + 1}{\pi + 2} & \dfrac{-2}{\pi + 2} \\ \dfrac{-1}{\pi + 4} & \dfrac{\pi + 1}{\pi + 2} \end{bmatrix} \begin{bmatrix} \chi_0 - s_y \\ \chi_1 - s_x \end{bmatrix}$$

And therefore, the value of the optimum R is available with respect to χ_0 and χ_1.

$$R = (\chi_0 - s_y)\left(\frac{3 + \pi}{(\pi + 4)(2\pi + 4)}\right) + (\chi_1 - s_x)\left(\frac{1}{\pi + 2}\right)$$

Another important restriction is that the distance between the center of the microchambers (D) should be more than the diameter of the microchambers plus a threshold for bonding considerations.

$$D = \sqrt{\chi_1^2 + (L - s_y)^2} > 2R + s$$

$$\chi_1^2 + (L - s_y)^2 > (2R + s)^2$$

Where s is minimum distance of the microchambers' wall with each other. Hence after designing the χ_0 and χ_1, the above inequality must be checked as well.

These considerations do not take care of other important conditions for separation. For example, one should be aware that w cannot be wider than tens of micrometers, otherwise the flow would change the stagnant condition of the microchambers during washing step. The geometries that we finally fabricated for testing the device are 6 different designs in the Table S1.

Table S1. The dimensions of the designs used for fabrication.

designs #	D [μm]	w [μm]	L [μm]	H [μm]	$s_x = s_y$ [μm]
1	350	60	521.48	30	70
2	350	60	521.48	70	70
3	500	60	521.48	30	70
4	500	60	521.48	70	70
5	1000	60	978.5	30	70
6	1000	60	978.5	70	70

2. SEM images of microchambers

The rough surfaces of the fabricated device may cause as random noise in the motion of sperm while swimming along the boundaries.

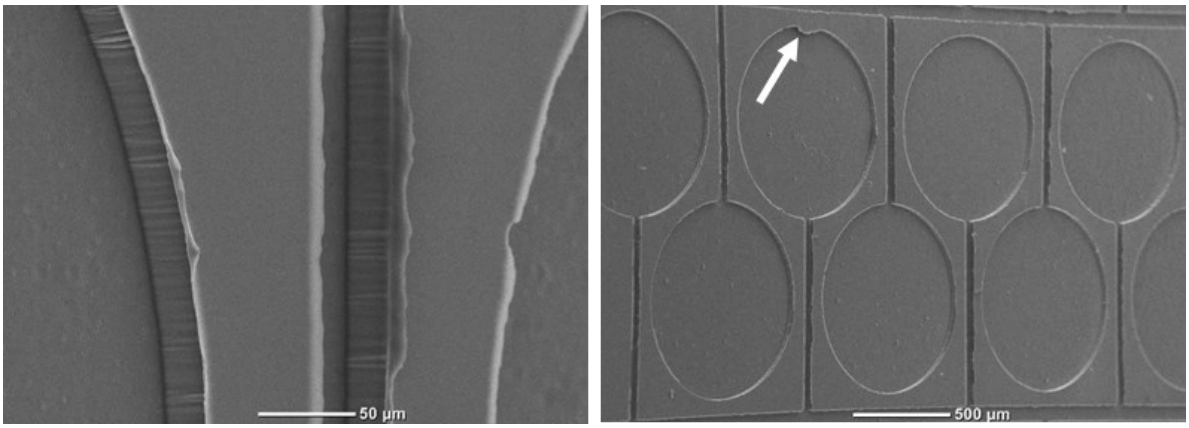

Figure S2. The SEM images with different magnification. The white flash shows a bump in the wall of the microchamber which cause random effects on the results of the experiments.

3. Theoretical Model of The Loading Time

Loading of the microchamber can be done though two different processes. First is to use constant pressure at the inlet (simply by exerting pressure on syringe plunge) and secondly, employing constant mass flow rate at the inlet. However, the main concept of the loading process remains the same. When fluid enters the microchamber the surface of the sample fluid and air trapped in the microchamber produce an angle with the walls of the microchamber which we assume to be constant and equal to the static contact angle. It holds true for a perfectly smooth wall, though due to the manufacturing randomness, the walls of the microchambers are rough. One of such a roughness and randomness of manufacturing is shown on Figure S2 with white flash. Therefore, it is one of the model's assumptions which result in errors against experimental data.

For both constant pressure and flow rate we presume that the main and connecting channels are filled with fluid and the solution starts as the fluid enters microchambers. Also, we assume that all microchambers are filled simultaneously with the same conditions; the fact that is roughly acceptable.

3.1. Constant Pressure

The pressure here means the pressure at the inlet and it differs from the air pressure trapped inside the microchamber by the amount of Laplace pressure. In this section p is the air pressure. Having said that one can write the correlation between inlet pressure and air pressure as it follows.

$$p_{in} = p + \frac{\sigma}{r}$$

For calculation of the loaded volume (V) over time we need to figure out how θ corresponds to the V.

In triangle OO'C:

$$\angle O'OC = \theta$$

$$\angle OO'C = \alpha - \theta$$

$$\angle O'CO = \pi - \alpha$$

The sin law gives us:

$$\frac{R}{sin\,(\alpha - \theta)} = \frac{r}{sin\,(\theta)}$$

Then it can be arranged as:

$$r = R\frac{sin\,(\theta)}{sin\,(\alpha - \theta)}$$

The volume of air based on the angle of θ is then calculated as

$$V = \left(\pi R^2 - \left\{\theta R^2 - \frac{1}{2}R^2 sin\,(2\theta) + (\alpha - \theta)r^2 - \frac{1}{2}r^2 sin\,(2\alpha - 2\theta)\right\}\right)H$$

In which H is the depth of the channel and we assumed a circular common interface of air and sample fluid since H is small compared to the radius of the microchamber.

Mass conservation indicates that the rate of the change of the mass of the air in the microchamber is equal to the amount of the air running form the porous media. We then assumed that the velocity of the air expelling from the boundary of the microchamber is a function of the pressure difference of the air inside (v(p)) and the fresh air outside of the

Polydimethylsiloxane (PDMS) device due to the Darcy's law. The combination of the abovementioned leads to:

$$\frac{d(\rho V)}{dt} = -\rho\left[(2\pi - 2\theta)HR + \left(\pi R^2 - \left\{\theta R^2 - \frac{1}{2}R^2 sin\,(2\theta) + (\alpha - \theta)r^2 - \frac{1}{2}r^2 sin\,(2\alpha - 2\theta)\right\}\right)\right]v(p)$$

Substituting V in the previous equation and assuming a constant pressure in the air inside microchamber gives:

$$\frac{d}{dt}\left(\frac{1}{2}R^2 sin\,(2\theta) + \frac{1}{2}R^2 sin\,(2\alpha - 2\theta) + (\alpha - \theta)r^2 - \frac{1}{2}r^2 sin\,(2\alpha - 2\theta)\right) = \left[2(\pi - \theta)R + \left(\frac{\pi R^2}{H} - \frac{1}{H}\left\{\theta R^2 - \frac{1}{2}R^2 sin\,(2\theta) + (\alpha - \theta)R^2 - \frac{1}{2}R^2 sin\,(2\alpha - 2\theta)\right\}\right)\right]V(p)$$

And thereafter we can get the differential of θ and r with respect to time.

$$H\left\{\dot{\theta}\left(R^2 - R^2 cos\,(2\theta) - r^2 + r^2 cos\,(2\alpha - 2\theta)\right) + \dot{r}(2r(\alpha - \theta) - r sin(2\alpha - 2\theta))\right\} = \left[(2\pi - 2\theta)HR + \left\{\left\{\theta R^2 - \frac{1}{2}R^2 sin\,(2\theta) + (\alpha - \theta)R^2 - \frac{1}{2}R^2 sin\,(2\alpha - 2\theta)\right\}\right\}\right]V(p)$$

The r is the first derivative of the radius r with respect to time which is calculated as below.

$$\dot{r} = R\frac{\dot{\theta} sin(\alpha)}{sin(\alpha - \theta)}$$

The abovementioned equation is a separable first order ordinary differential equation with initial condition of $\theta=\theta_0$ that is the angle of the inlet of the microchamber.

3.2. Constant flow rate

As in the case of constant pressure the volume of the TALP inside the microchamber is

$$V = \left\{\theta R^2 - \frac{1}{2}R^2 sin\,(2\theta) + (\alpha - \theta)r^2 - \frac{1}{2}r^2 sin\,(2\alpha - 2\theta)\right\}H$$

Which changes by the rate of flow inside the microchamber and *r* is the same as the constant pressure case.

$$\frac{dV}{dt} = \frac{\dot{m}}{N\rho_f} = \frac{\dot{Q}}{N}$$

In which ρ_f is the fluid density, $\dot{m}$ is the mass flow rate at the inlet and N is the total number of the microchambers.

This derivation and formula are not in the main concern of the paper and needed some extra devices to make to be validated and so we ignored about their validity but in the supplementary Movie 1 we showed that they qualitatively provide an explanation for the loading profile of the microchambers for depth of 30 μm. For higher depth, this formulation needs some modification regarding the interface of the sample which can no longer be assumed as a 2D curved face rather it resembles a part of a sphere surface.

3.3. Loading Results.

Loading of the microchambers in our experiments have not been done with constant pressure nor constant mass flow rate. When we filled the main channels with the sample, we blocked the outlet and turned on the syringe pump with different flow rates. When the flow starts to fill the microchambers the pressure in the microchambers increase and then in order to keep the flow rate the pump increases the pressure at the inlet. Therefore, it is not possible to report any specific pressure at the inlet except that by increasing the flow rate the pressure increases up to a threshold in which it could be detrimental for the pump. Hence, we chose two safe flow rates of 1240 μL h^{-1} and 540 μL h^{-1} (Figure S3)

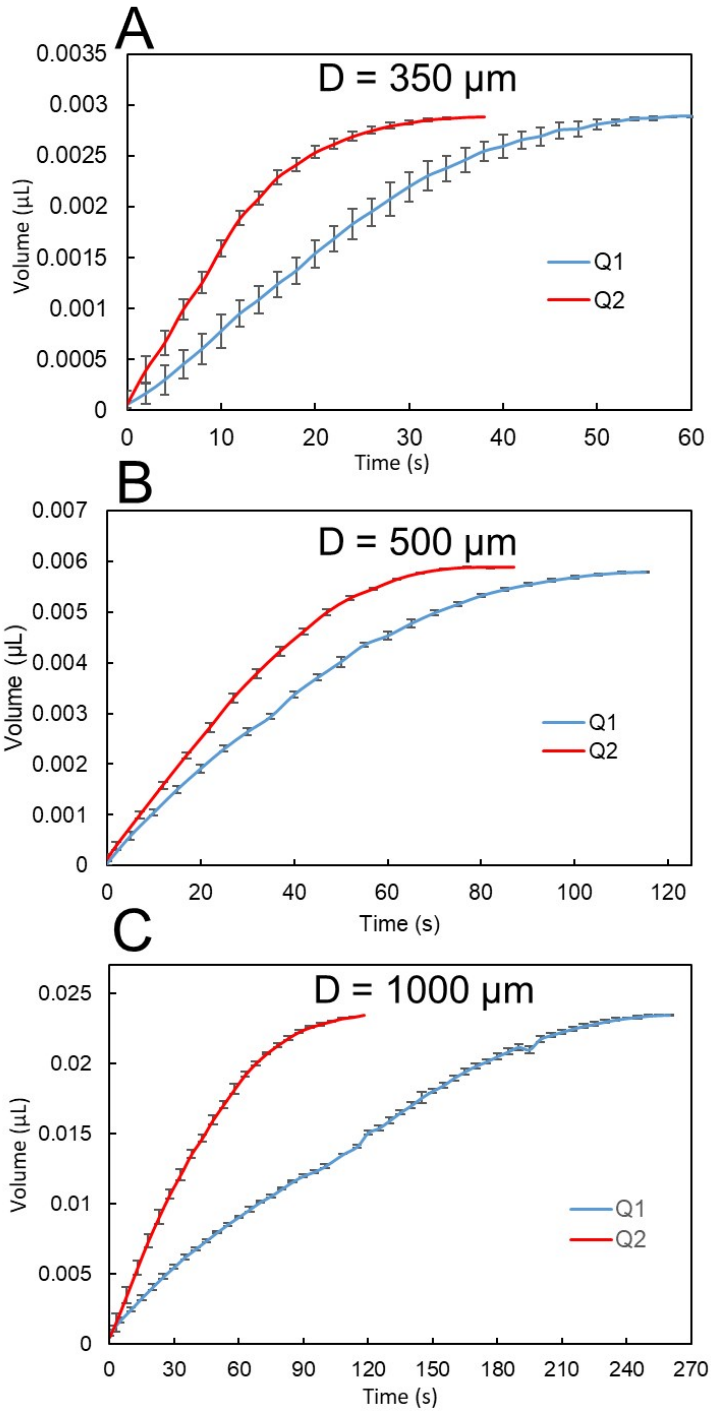

Figure S3. Loading volume of samples in the microchambers with different diameters for the depth of 30 μm. Q_1=540 μL/h and Q_2 = 1240 μL/h. (A) is for 76 microchambers, (B) is for 48 microchambers and (C) is for 36 microchambers.

4. Rheotaxis of the sperms in the main channel.

Rheotaxis occurs when sperms come out of the microchambers and are exposed to the shear rate in the main channel resulting from the velocity gradient. The rate at which the tail of the sperm is rotated in the flow is proportional to the sinus of the angle of tail with the direction of the flow[1]. The angles and the flow direction are shown in the Figure S4.

$$\frac{d\theta}{dt} = -A\gamma sin(\theta)$$

In which γ stands for the shear rate and A is a dimensionless empirical constant which is different for various kinds of swimmers(2). In our case we assumed A to be 0.07.

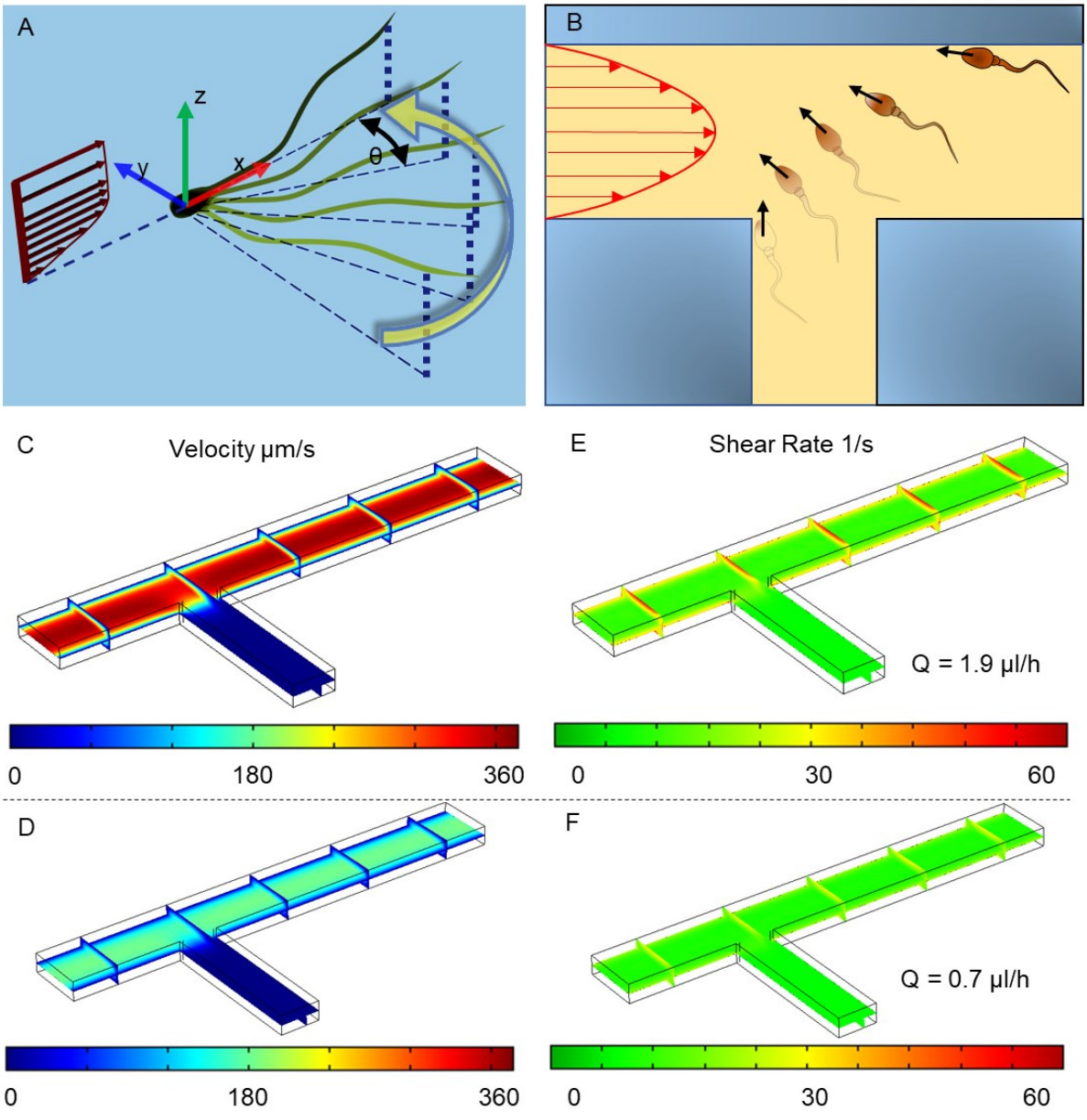

Figure S4. (A,B) Schematic diagrams of rheotaxis in 3D and 2D view. (C,D) the velocity magnitude and (E,F) the sear rate contours in the junction for two different flow rates in main channels with the same color map for each column on series of cut plains.

Mathematically speaking, sperms are supposed to be dots which can swim with v_{sperm} in the non-flow condition and therefore their trajectories is calculated by solving ordinary differential equation of lumped particles privileged by a propulsive force of their tails proportional to v_{sperm}. The sperm's size for bovine and human does not exceed 10 μm and hence they can be carried away by the flow from stagnant state in about 3 μs. Therefore, we assumed that the sperm velocity is simply the net resultant of fluid velocity and the velocity resulted from the motion of the flagella.

$$\frac{\vec{dr}}{dt} = \vec{v}_{sperm} + \vec{u}$$

$\vec{u}$ in the above equation stands for fluid velocity vector near the top surface (z = 22 μm) and $\vec{v}_{sperm}$ applies the propulsive velocity of sperms in its direction of movement (θ) and r shows the vector of sperm position with respect to initial position in the domain. Another assumption that will lead to equation of sperm's trajectories is that the sperm's average density is equal to density of the fluid otherwise the buoyancy would affect their positions.

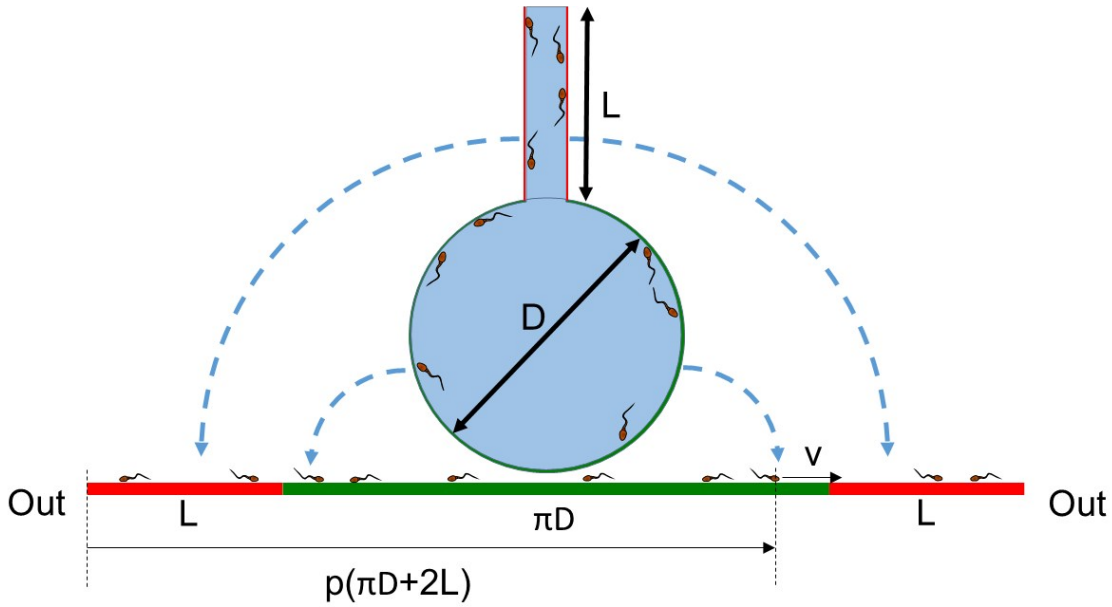

Figure S5. Illustration of the residence time in a congruent mapping of the microchambers boundaries on a line with same length.

At initial step, the position of the sperm are at the point with 2.5 μm distance from the corner at each wall. v_{sperm} are a normal distribution with mean 80 μm/s and variance 20 μm/s and $u(t=0)$=80 μm/s for all of the 20 sperms at each side. The fluid in the main channel in the collection step is TALP which can be considered as Newtonian fluid with viscosity and density of water. We used default "water-liquid" in COMSOL 5.4a (ρ = 1000 kg/m^3 and μ = 0.001003 Pa.s).

The fluid velocity, pressure and shear rate were solved in a 3D design as shown in Figure S4C-F and then the 2D velocities and shear rates imported in a 2D model for solving the rheotaxis dynamics of sperm. The trajectories of the sperm in the junctions for two flow rates are shown in Figure 4B in the main text.

5. Residence time distribution model

Expansion of the boundaries of the microchamber to a congruent line of three parts with the length equal to the periphery of the microchamber and connecting channel walls. The position

of each sperm on the wall is identical to its position on the line. This assumption is raised from the observations that sperms mostly remain on/near the walls (Figure S5).

As the diameter of the microchambers increases, and more volume is loaded in the microchambers, the sperm-sperm interaction becomes more important in the calculation of the residence time, however, this effect is not considered in this model. Furthermore, as shown in the Figure S2, some bumps and fabrication-related surface roughness, interferes with boundary navigation and speed of the sperms. Therefore, by increasing the diameter of the microchambers, the theory deviates more from experiment.

The time profile of the sperm count for different depth and different microchamber diameters are shown in the Figure S6. The fact that the number of sperms in each microchambers differs in different trails is due to inhomogeneity of the sample. To evaluate the retrieving efficiency in the next part we counted the number of sperms being extracted from a specific row in the hope that these numbers would be consistent. More elaborate model with detailed simulation of active particles can be found elsewhere using similar design.(3)

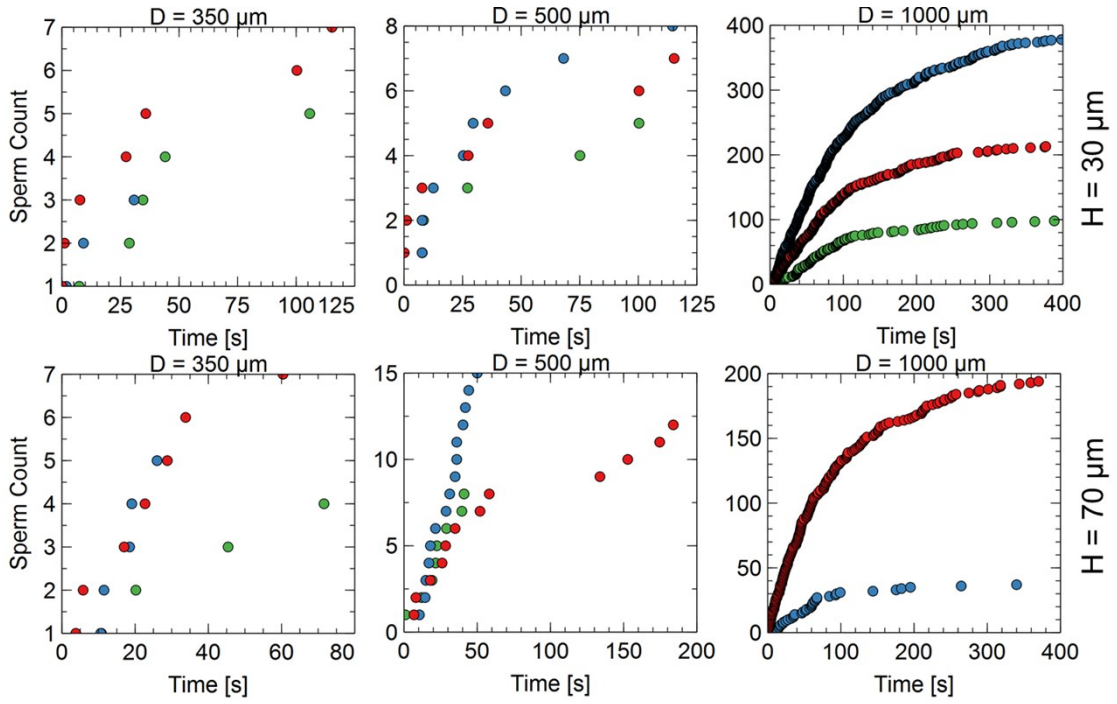

Figure S6. The time profile of the number of the sperms exiting the same microchamber in each diameter and depth of the chip for 3 trails (each color shows one trail). The sample concentration is 8M mL^{-1} with 13% motile sperms.

6. Trapping nonprogressive sperm

Nonprogressive sperm in the D = 1000 μm and depth 70 μm are trapped in the microchambers and after about ~ 15 minutes washing, crater-like holes appear in the microchambers. Figure S7 shows these moon crater-shaped holes and how they are created by motion of nonprogressive sperm over time. The egg yolk extender particles are deviated to the outside of the circle of motion of sperm since the asymmetric motion of the tail generates a centrifugal force on the fluid that will push particles away from the center.

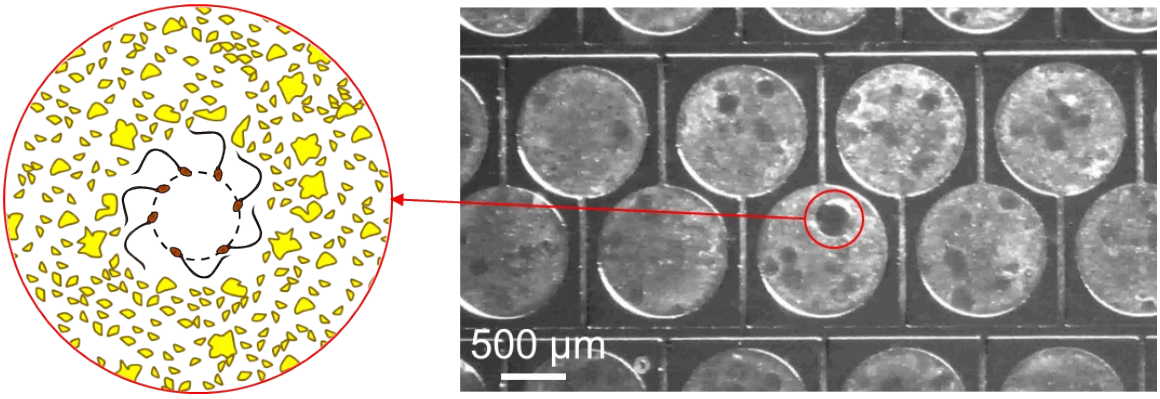

Figure S7. Trapping of nonprogressive spermatozoa creates moon crater-shaped hollows in the microchambers.

7. Effect of the escape gap size in various designs

We hypothesized that the wider the gap size per loaded volume the higher the chances are for the sperm to escape from the loading area to the collection area. The data in Table S2 is presented to show that hypothesis may be true even though the type of sperm being used in these works are not the same.

Table S2. Comparison of the escape gap size for different platforms of sperm separation.

designs #	Loaded Volume [μL]	Gap Area [m^2]	Separation Time [min]	Area per Volume [m^2/m^3]	Sperm Type	Recovery %
Ref [18]	1000	0.00000375	60	3.75	Human	-
Ref [14]	560	3.927×10^{-5}	60	70.12	Human	~40
Microchambers	21	1.613×10^{-6}	5	76.8	Bovine	~75

Other Files:

Movie S1. Qualitative simulation of common interface of injected fluid and air trapped in the microchamber. This is for case D = 350 μm and 30 μm depth and Q = 540 μL/h.

Movie S2. The position of nonviable sperm and debris is not affected by washing the main channels.

Movie S3. Rheotaxis of sperm exiting a microchamber for two washing flow rates of Q = 0.7 μL/h and 1.9 μL/h.

Movie S4. Collection of sperm by washing main channels in D = 1000 and depth of 70 μm design.

Movie S5. The extracted sperm from D = 1000 and depth of 70 μm design and control sperm sample.

SI References

1. Zaferani M, Cheong SH, Abbaspourrad A. Rheotaxis-based separation of sperm with progressive motility using a microfluidic corral system. Proceedings of the National Academy of Sciences. 2018;115(33):8272-7.
2. Tung C-k, Ardon F, Roy A, Koch DL, Suarez SS, Wu M. Emergence of upstream swimming via a hydrodynamic transition. Physical review letters. 2015;114(10):108102.
3. Paoluzzi M, Angelani L, Puglisi A. Narrow-escape time and sorting of active particles in circular domains. Physical Review E. 2020;102(4):042617.